

Developments on the Sliding Hinge Joint

H. H. Khoo, G. C. Clifton & J. W. Butterworth

University of Auckland, New Zealand

G. A. MacRae

University of Canterbury, New Zealand



SUMMARY:

This paper provides a review of the Sliding Hinge Joint (SHJ), asymmetric friction connection (AFC) and self-centering SHJ (SCSHJ). The SHJ is a low damage beam-column connection that is rigid under serviceability level conditions and rotates under design level earthquake shaking through sliding in AFCs. The AFC decouples joint strength and stiffness, and confines inelastic demand to the bolts. The SHJ is nevertheless subject to residual drifts and elastic strength losses. Experimental testing on the AFC has shown improved performance with abrasion resistant steel shims. The sliding friction capacities are determined through a model based on plastic theory. This is because the bolts are subject to the interaction of moment-shear-axial forces during sliding. The SCSHJ incorporates ring springs as a self-centering component, designed as a percentage of total joint moment capacity (P_{RS}). Analytical studies showed reduced frame residual drifts with increasing P_{RS} . Experimental tests showed improved flag-shape response with increasing P_{RS} .

Keywords: Self-centering; friction; beam-column connection; moment resisting frame; low-damage

1. INTRODUCTION

The Sliding Hinge Joint (SHJ) is a beam-column connection used in steel moment resisting frames (MRFs). It was initially developed by the New Zealand Heavy Engineering Research Association (HERA) and the University of Auckland from 1998 to 2005 (Clifton, 2005) as a low-damage alternative to traditional welded connections.

The SHJ (Fig. 1.1) pins the beam to the column through the top flange plate, with asymmetric friction connections (AFCs) in the bottom web and flange bolt groups that slide during joint inelastic rotation. The use of the AFC decouples joint strength and stiffness, and confines inelastic demand to the bolts. Under inelastic rotation, the beam rotates about the top flange plate, which eliminates beam growth and minimises interaction with the floor slab. The SHJ is designed to be rigid under working load and serviceability level conditions, rotate through sliding in AFCs under the design level earthquake (DLE) shaking, and return to effectively rigid at the end of the earthquake shaking. Its benefits over rigid connections include (1) decoupling of moment frame strength and stiffness which enables larger beam sizes without imposing high overstrength demands on the columns, (2) confining inelastic demand to the bolts, (3) improved seismic-dynamic recentering ability, (4) lower cost.

The SHJ is, however, subject to elastic strength and stiffness losses during inelastic rotation. This is because the bolts in the AFC undergo further plasticity during sliding, which reduces the bolt clamping force. Furthermore, the SHJ does not have a self-centering mechanism and may be subject to residual deformation. This paper provides a review of the next stage of the SHJ development, the main objective of which is to provide reliable self-centering ability and minimal losses in elastic strength and stiffness. This paper provides a description of the SHJ, developments on the AFC, and the development of the self-centering Sliding Hinge Joint (SCSHJ).

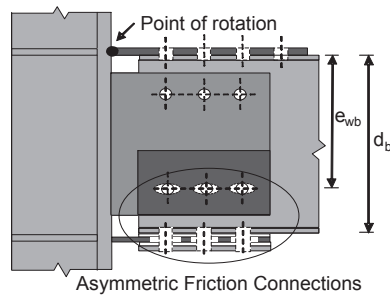


Figure 1.1. SHJ layout (MacRae et al., 2010)

2. SLIDING HINGE JOINT

The top corner of the beam is pinned to the column through the top flange plate. Under seismic moment demand, the SHJ remains rigid until the sliding resistance provided by the web bottom and bottom flange AFCs is exceeded. The AFCs then start to slide, allowing joint inelastic rotation, while confining yielding to the bolts. Fig. 2.1 shows the rotation of the SHJ, and the idealised moment-rotational behaviour. The components of the AFC in the bottom flange (labelled in Fig. 2.1a) consist of a cleat welded to the column coming into the beam, and sandwiched between the beam flange and cap plate. The web plate AFC likewise consists of the beam web and cap plate sandwiching the web plate. The cleat and web plate have elongated holes to allow sliding, with nominal sized bolt holes in the other components. Shims are inserted in-between sliding surfaces, on which sliding takes place. The bolts are Property Class 8.8, which are tensioned into the inelastic range during installation by the turn of nut method, in accordance with the Steel Structures Standard, NZS 3404 (Standards New Zealand 2009).

The AFC has two sliding surfaces. The first is the cleat/web plate and the upper/inner shim interface, and the second is the cleat/web plate and the lower/outer shim plate interface. When the static frictional resistance of one surface is exceeded, the first interface slides, shown as (b) in Fig. 2.1c. As the demand increases, the second interface slides, approximately doubling the frictional resistance as shown as (c). Under load reversal, the AFC has a near zero moment before building up. Sliding occurs initially on the first interface (d) followed by the second (e). This results in a “pinched” hysteresis curve, which gives a self-centering tendency to the SHJ.

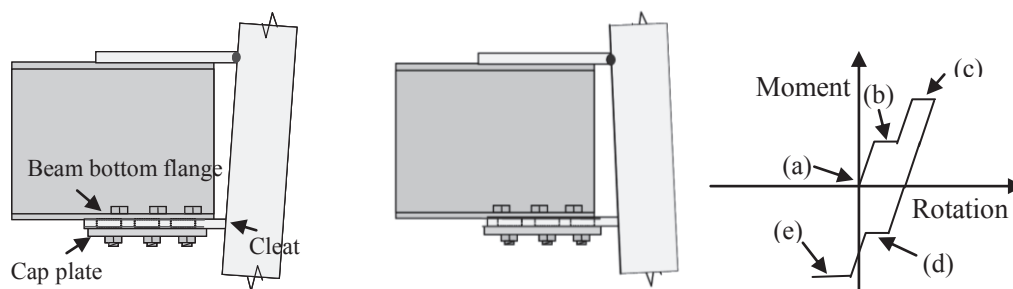


Figure 2.1: SHJ (a) negative rotation, (b) positive rotation and (c) idealised moment-rotation behaviour (MacRae et al., 2010)

3. DEVELOPMENTS IN THE ASYMMETRIC FRICTION CONNECTION

The AFC is a key component of the SHJ and its application in other seismic resistant systems has also been proposed (Khan and Clifton, 2011, Chanchi-Golondrino et al., 2012). The AFC behaviour is dependent on the shim material and the axial force over the two sliding surfaces. Research has been undertaken to develop better performing and cheaper AFCs addressing these two issues.

3.1. Shim Material

Brass shims were tested in the original development of the SHJ (Clifton, 2005). This was in accordance with the findings of Grigorian and Popov (1994), who reported force fluctuations in symmetric sliding between mild steel surfaces, and stable sliding between mild steel and brass. Testing at both quasi-static and dynamic rates of loading in the SHJ produced stable sliding characteristics, and brass was therefore recommended. There are however cost, availability and corrosion issues with brass against steel.

MacRae et. al (2010) then compared aluminium, mild steel and brass shims in three-quarter scale beam-to-column SHJ subassembly tests at quasi-static rates of loading. It was found that mild steel and brass shims exhibited similar moment-rotation behaviour and capacity. It was postulated that this was due to asymmetric sliding eliminating peaks, as compared to symmetric sliding (Grigorian and Popov, 1994). Mild steel shims are cheaper, more readily available, eliminate dissimilar metal corrosion issues at the interface, and can be tack welded in place. They have since been adopted in SHJ building construction.

Khoo et. al (2012a) tested steel shims of different grades, with the understanding that sliding between surfaces of different hardness improves performance. The tests were undertaken at dynamic rates of loading with boundary conditions similar to the SHJ. Fig. 3.1 presents the force-displacement curves of mild steel and low alloy abrasion resistant steel shims (Bisalloy Steels, 2008). The measured hardness of the shims was 168 HB and 382 HB respectively in the Brinell scale. Abrasion resistant steel performed the best with the highest frictional resistance, the least wear and the most stable curves. While slightly more expensive than mild steel, they give demonstrably better performance and the same benefits as mild steel over brass. They have been recommended for use in future construction.

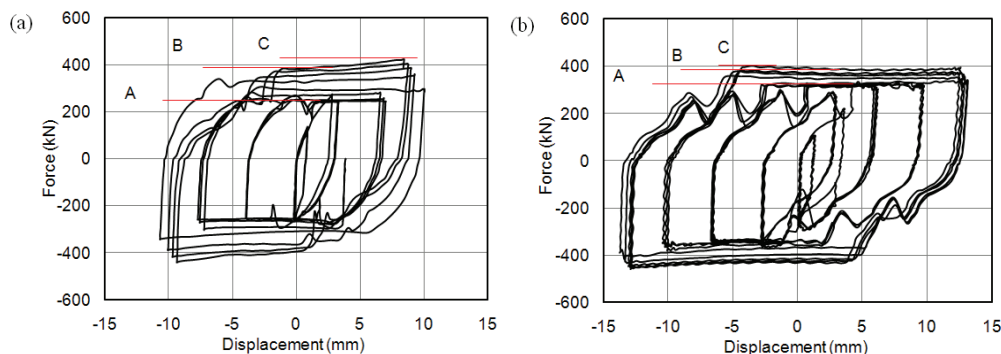


Figure 3.1. Force-displacement characteristics of (a) mild steel shims and (b) abrasion resistant steel shims (Khoo et al., 2012a)

3.2. Sliding Capacity

The AFC frictional resistance is the product of the coefficient of friction (μ) between the sliding surfaces (ie. dependent on shims), and the bolt axial tension (N). Due to asymmetric sliding, the bolt axial tension is dependent not just on the initial installed bolt tension, but the interaction of moment-shear-axial forces (MVN) during sliding, which generates further plasticity in the bolts which installed beyond their yield point. The MVN is a function of the lever arm between the forces acting on the bolt and resulting moment distribution. This results in an uneven stress distribution in the cross-sectional area of the bolt, and a drop in the installed tension. It is also this drop in tension which causes the SHJ to lose elastic strength and stiffness once forced into the sliding state. Fig. 3.2 shows the idealised deformation, free body diagram, and moment distribution on the bolt.

The sliding shear capacity (V_{ss}) used in design is therefore calculated by a model based on plastic theory initially developed by Clifton (2005), and modified by MacRae et. al (2010). It captures the

effects of the MVN, and computes the V_{ss} based on the bolt proof load (N_{tf}), μ , and the cleat thickness. The μ adopted is 0.29 and 0.30 for brass and steel respectively, with computed values comparable to lower bound experimental test results for both shims. The model is summarised in Eqns. 3.1 to 3.5. It should be noted that for abrasion resistant steel shims, the point of contact is between the shims and the bolts as opposed to the cleat and cap plate as shown in Fig. 3.2. This changes the lever arm (l) to the distance between shim to shim (Khoo et al., 2012a).

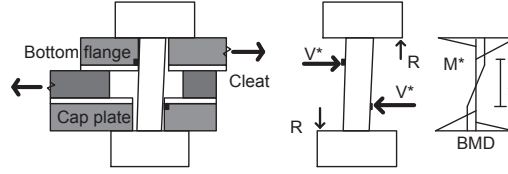


Figure 3.2. Idealised deformation, free body and bending moment diagram on AFC bolt (MacRae et al., 2010)

$$\frac{M^*}{M_{rfn}} + \frac{V^*}{V_{fn}} < 1 \quad (3.1)$$

$$V^* = N\mu \quad (3.2)$$

$$M^* = \frac{V^* l}{2} = \frac{N\mu l}{2} \quad (3.3)$$

$$M_{rfn} = S_{fn} \left(1 - \left(\frac{N}{N_{tf}} \right)^c \right) f_{uf} \approx 0.1665d^3 \left(1 - \left(\frac{N}{0.56d^2 f_{uf}} \right)^c \right) f_{uf} \quad (3.4)$$

$$V_{fn} \approx 0.62 f_{uf} \times 0.56d^2 \quad (3.5)$$

where: M^* = bolt moment demand; M_{rfn} = bolt moment capacity considering axial force interaction; V^* = shear force carried by each bolt; V_{fn} = bolt shear capacity considering no axial force interaction; N = bolt tension during sliding; l = lever arm and taken as cleat thickness + 2×shim thickness + 0.2d for brass and mild steel shims, and taken as cleat thickness + 0.2d for abrasion resistant steel shims; S_{fn} = plastic section modulus of the circular core area; f_{uf} = 830 MPa (bolt ultimate tensile stress); d = nominal bolt diameter; c = constant which is taken as 1 without Belleville springs and 2 with Belleville springs.

4. SELF-CENTERING SLIDING HINGE JOINT

The self-centering SHJ (SCSHJ) was proposed to reduce residual deformation and losses in elastic strength. The SCSHJ aims to ensure the building is fully operational following a DLE shaking, through the use of friction damping ring springs manufactured by Ringfeder, Germany (Ringfeder GmbH, 2008). Ring springs consist of inner and outer rings with tapered surfaces, which deform through sliding between the tapered surfaces. They can therefore only be loaded in compression, where 66% of the energy is dissipated through friction, with the remainder stored as elastic energy in the outer and inner rings. The SCSHJ has been studied analytically (Khoo et al., 2012c) and experimentally (Khoo et al., 2012b).

4.1. Joint Description

The SCSHJ combines the behaviour of the SHJ, with the self-centering flag-shaped behaviour of a dual-directional prestressed ring spring cartridge connected to the beam bottom flange and column flange. Fig. 4.1 shows a schematic drawing of the SCSHJ layout and ring spring cartridge assembly. The ring spring cartridge configuration is required to ensure the spring deforms in compression regardless of loading direction. It consists of a threaded bar and nuts, endplates, and a housing cage. The bar is fixed to the column shown as C (Fig. 4.1a). The bar transfers load from the column to the

endplates, which then compresses the ring spring. The housing cage is a rectangular box that houses the ring spring. It determines the level of ring spring prestress when the joint is at rest, and prevents the spring from buckling during compression. When a positive moment is applied, the SCSHJ remains rigid till the combined AFC resistance and ring spring prestress is exceeded. The column then rotates away from the beam through sliding in the AFCs, pulling the bar, and opening a gap between endplate A and the housing cage interface. Endplate B bears on the other end of the cage, forcing the ring spring to compress. Under negative moment, the column pushes the bar towards the beam, opening a gap between endplate B and the cage, again compressing the ring spring. The ring spring cartridge configuration is dual-directional acting, and is similar to a ring spring seismic damper proposed and tested by Filiatrault et. al (2000). They reported stable and repeatable force-displacement characteristics with minimal degradation. Shake table tests and numerical studies on a single storey braced frame showed effective energy dissipation and reduced lateral displacements and accelerations. The ring spring changes the SHJ behaviour in three ways, namely: (1) contributes to moment resistance and reduces the required number of AFC bolts, which reduces the frictional resistance to recentering, (2) energy stored in the spring contributes to the recentering restoring force upon load reversal/removal, and (3) ring spring prestress reduces loss in joint elastic strength or stiffness as it does not undergo degradation.

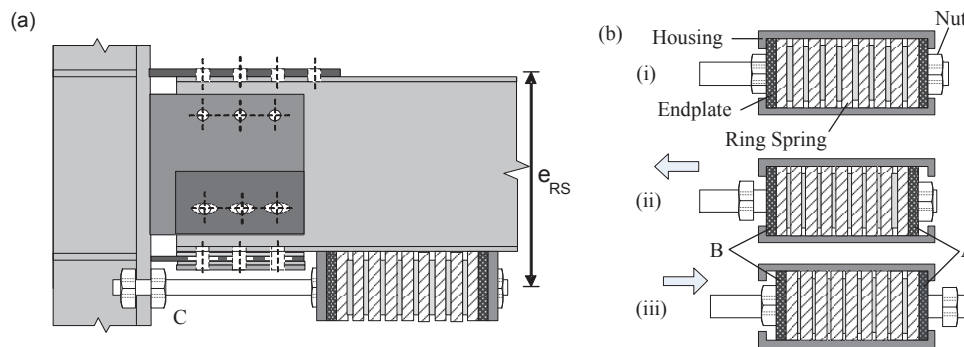


Figure 4.1. (a) SCSHJ layout and (b) ring spring layout

Fig. 4.2a shows the idealised moment-rotation behaviour of the standard SHJ, including load history dependence. At low amplitudes, the resistance is lower as the AFC requires sufficient sliding distance to develop full capacity. Fig. 4.2b shows the theoretical moment rotational behaviour of the Ring Spring Joint (RSJ). The RSJ is defined as the joint with only ring spring contribution and exhibits the ideal flag-shape self-centering hysteretic behaviour. The SCSHJ behaviour is shown in Fig 4.2c. It is a combination of the SHJ and RSJ, and is best suited for drift control and self-centering. Drift control is achieved through high strength and energy dissipation in the first and third quadrants of the hysteresis curve, while self-centering capability is achieved through minimal strength in the second and fourth quadrants. The SCSHJ with a significant AFC contribution to strength does not reflect the flag-shaped hysteresis curves typical of some self-centering systems, such as post-tensioned steel tendon (Ricles and Sause, 2001) and shape memory alloy systems (Ocel et al., 2004). These systems develop static recentering properties, where the connections return the frames to their original plumb position when the load is released slowly from the design displacement. In reality, structures are subject to seismic dynamic effects, which results in reduced the residual displacements due to shake-down effects (MacRae and Kawashima, 1997). The objective of the SCSHJ is to improve the seismic-dynamic recentering properties to a dependable level, taking these effects into account.

The SHJ has been shown (Clifton, 2005) to have a tendency to recenter. This is due to the “pinched” curve as described in Section 2, and high post-elastic stiffness (MacRae and Kawashima, 1997). The ring springs further improve the performance by increasing the “pinch” as shown in Fig. 4.2c. In addition to that, the performance is improved due to the reduction in AFC resistance under lower amplitude cycles, as the AFC requires sufficient sliding distance to develop the full resistance of both sliding surfaces. The ring spring resistance is unchanged, which would then dominate the joint rotation characteristics, and thus improve the flag-shape curve during shake-down.

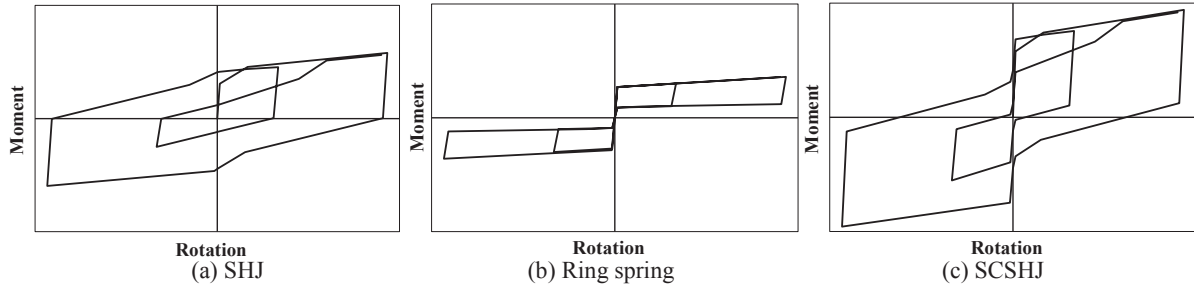


Figure 4.2. Idealised hysteretic behaviour

4.2. Self-centering Sliding Hinge Joint Design

The SCSHJ is designed based on a target percentage (P_{RS}) of total moment capacity developed by the ring springs. A joint with a $P_{RS} = 0\%$ equates to the standard SHJ with no ring spring contribution, while a $P_{RS} = 100\%$ equates to the RSJ where there is no AFC contribution. The design of the joint is summarised in Eqns. 4.1 to 4.5.

$$M_{SHJ} = n_{wbb}V_{ss}e_{wb} + n_{bfb}V_{ss}d_b \quad (4.1)$$

$$M_{RS} = F_p e_{RS} \quad (4.2)$$

$$M_{SCSHJ} = M_{SHJ} + M_{RS} \quad (4.3)$$

$$M_{RS} = P_{RS} M_{SCSHJ} \quad (4.4)$$

$$P_{RS} = \frac{M_{RS}}{M_{SCSHJ}} \times 100 \quad (4.5)$$

where M_{SHJ} = AFC moment contribution; n_{wbb} = number of bolts in the bottom web AFC; n_{bfb} = number of bolts in the bottom flange AFC; e_{wb} = bottom web AFC lever arm (as shown in Fig. 1a); V_{ss} = sliding shear resistance per bolt; n_{bfb} = number of bolts in the beam bottom flange AFC; d_b = beam depth; M_{RS} = ring spring moment contribution; F_p = ring spring pre-compression; e_{RS} = ring spring lever arm (as shown in Fig. 2a); M_{SCSHJ} = SCSHJ moment.

5. ANALYTICAL STUDIES

Time history analyses were undertaken on five, 5-bay, 10-storey MRFs to determine the effects of different levels of P_{RS} (Khoo et al., 2012c). The frames were based on the Te Puni Village Tower Building in Wellington, New Zealand (Gledhill et al., 2008), which was built using the standard SHJ. The building was designed in accordance with New Zealand loading and steel standards (Standards New Zealand, 2004a). The joints in the frames were designed with target P_{RS} of 0%, 15%, 25%, and 40%. The frames were studied with 10 ground motions (Oyarzo-Vera et al., 2012), which were scaled to the 500 year return period DLE. The extent of damage was evaluated with the peak interstorey drift (δ_p), with a damage threshold of 2.5% (Standards New Zealand, 2004a). The maintenance required following the earthquake was evaluated with the residual interstorey drift (δ_r), with a damage threshold of 0.1%.

5.1. Peak and Residual Drift Response

Fig 5.1. presents δ_p and δ_r results with respect to the different levels of P_{RS} . It presents the mean as well as the distribution of individual ground motions. There was little difference in the mean δ_p , which was between 1.54 and 1.58% for frames with P_{RS} of 0 to 40%. The distribution of δ_p under the individual ground motions was also similar, which indicated that joint P_{RS} is independent on frame displacement demands.

The frame with P_{RS} of 0% (ie. the standard SHJ), had the highest residual drift, with a mean δ_r of 0.12%, and the largest number of ground motions exceeding damage thresholds. The residual deformation then reduced with increasing P_{RS} . The mean δ_r was 0.07%, 0.05% and 0.04% for P_{RS} of 15%, 25% and 40% respectively, showing the ring springs improved the dynamic self-centering abilities of the joint. The frames with P_{RS} of 40% were under the damage threshold of 0.1% for all ground motions. There was a disproportionate benefit with increasing P_{RS} . This is seen in comparing the reduction of residual deformation from P_{RS} of 0% to 15%, and from P_{RS} of 25% to 40%. The former improved the performance more significantly with a reduction in mean δ_r of 0.05%, compared to 0.01% in the latter. While the performance improved with increasing P_{RS} , it was not to the same effect as the initial increase from P_{RS} of 0 to 15%.

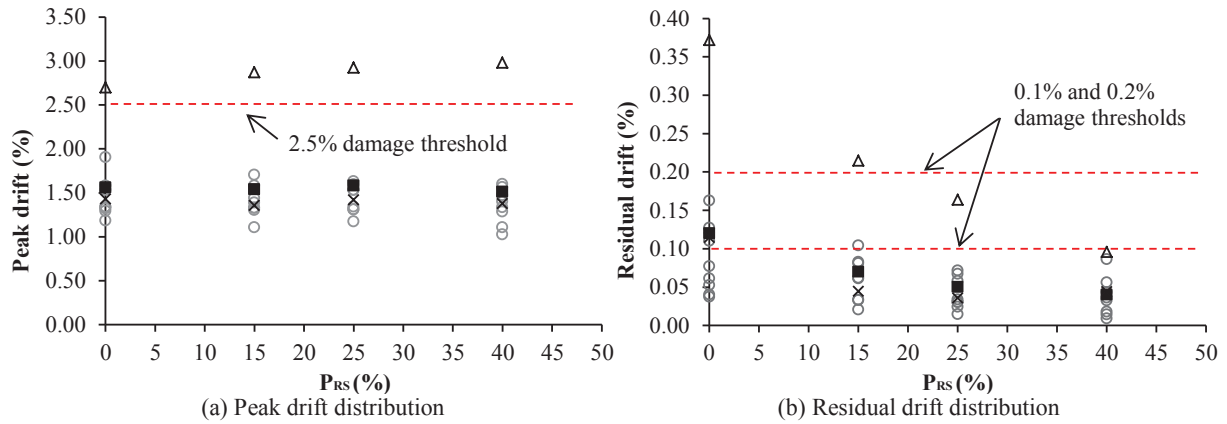


Figure 5.1. Effects of P_{RS} on peak and residual drifts (Khoo et al., 2012c)

5.2. Moment-rotational behaviour

Fig. 5.2. compares the hysteresis response of joints with P_{RS} of 0% and 40% under the time-history analyses. The curves were shown to better resemble flag-shaped curves as the P_{RS} increased. As noted above, the P_{RS} investigated was insufficient to develop full static recentering. The effectiveness of the ring springs is nevertheless shown by the near zero residual rotation in the $P_{RS} = 40\%$ joints, despite lacking the full flag-shaped self-centering curves. As described in Sections 2 and 4.1, the AFC resistance is load history and amplitude dependent, and requires sufficient sliding distance to develop the full capacity of two sliding surfaces. The amplitude decreases during shake down which lowers the AFC sliding resistance (shown as ΔV in Fig. 5.2.a), while the ring spring resistance is unchanged. This increase in effective P_{RS} with decreasing amplitude then enhances the flag-shape and self-centering characteristics of the joint (Fig. 5.2.b).

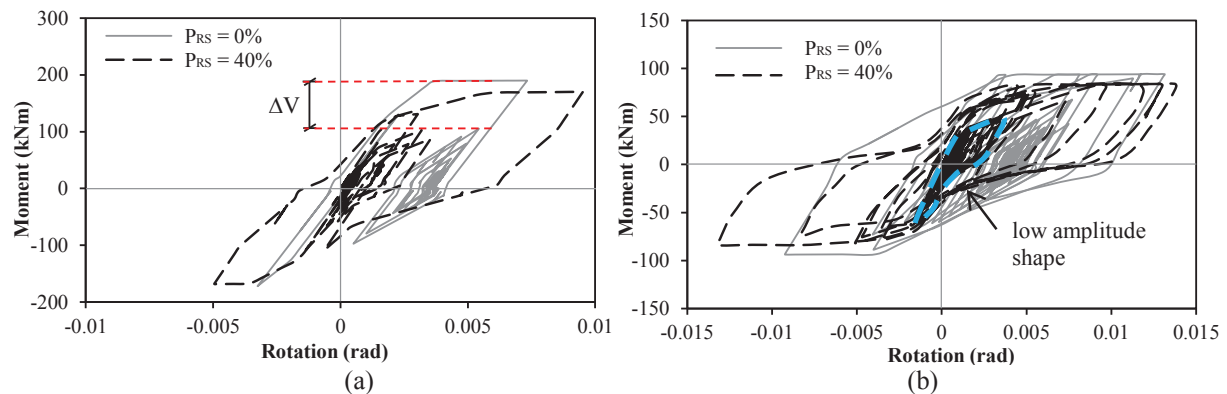


Figure 5.2. Effects of ring springs on the hysteresis behaviour of the SCSHJ: (a) storey 8 joint under El Centro 1979 DLE and (b) storey 9 joint under Tabas MCE (Khoo et al., 2012c)

6. EXPERIMENTAL STUDIES

6.1. Test description

Experimental tests were undertaken on full-scale SHJ and SCSHJ subassemblies with different levels of P_{RS} (Khoo et. al 2012b). The test setup is shown in Fig. 6.1.a, and simulated an internal connection in on the 8th floor of the Te Puni Village Tower Building MRF (Gledhill et al., 2008). A steel deck concrete slab (Fig. 6.1.b) was installed to test the ability of the joint to isolate the floor slab, and to determine the likely level of damage after an earthquake. The column stiffener configuration (Fig. 6.1.c) allowed the RS bar to be connected to the column flange. The loading regime adopted was recommended by the SAC Joint Venture (2000) for steel MRF connection subassembly tests, which consisted of stepwise increases in drift (δ). It was six cycles of $\delta = 0.375\%$, 0.5% , and 0.75% , four cycles of $\delta = 1\%$ and two cycles of $\delta = 1.5\%$, 2% and 3% at quasi-static rates of loading.

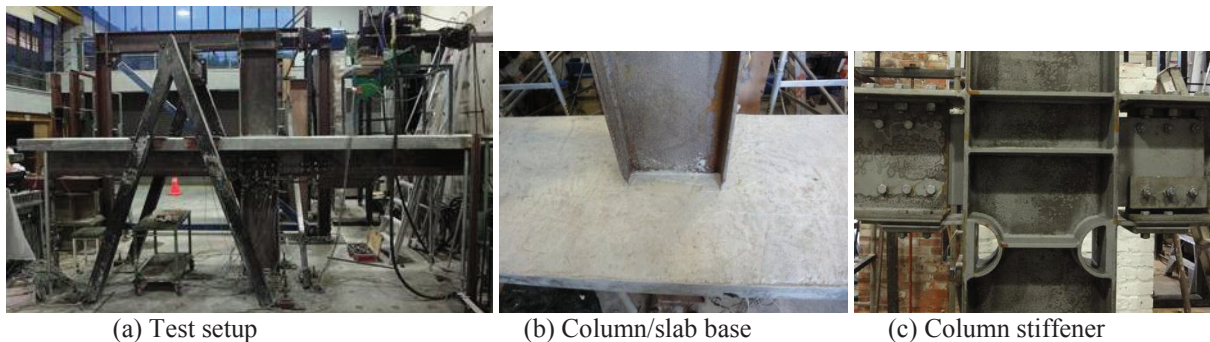


Figure 6.1. Test figures

6.2. Specimens

The specimens were designed to P_{RS} of 0% , 20.5% , 40.2% , 52.6% , and 100% . The same column, beams and slab was use for all tests, with the AFC and ring spring assembly varied to the desired P_{RS} . Two ring spring cartridges were tested. They were Type 08000, and Type 12400. The housing cage for one of the Type 08000 cartridges is shown in Fig. 6.2a. The cartridge was assembled and installed in the SCSHJ with the following steps: (1) ring spring with endplates on each end inserted in the housing through the open end (unstressed ring spring is longer than the housing), (2) prestressing bar inserted through the ring spring and nuts tightened on each end, (3) ring spring compressed through a jack pulling the bar from the closed end of the housing till the ring spring is shorter than the housing length, (4) cover plate bolted over the free end of the housing, (5) pressure in the jack is released till the ring spring prestress is held by the housing, (6) bar and nuts removed, (7) cartridge bolted onto the bottom flange of the beam, (8) threaded bar inserted through the cartridge and into the column, and (9) nuts tightened around the column flange and cartridge. Fig. 6.2c shows the SCSHJ with Type 08000 cartridge.

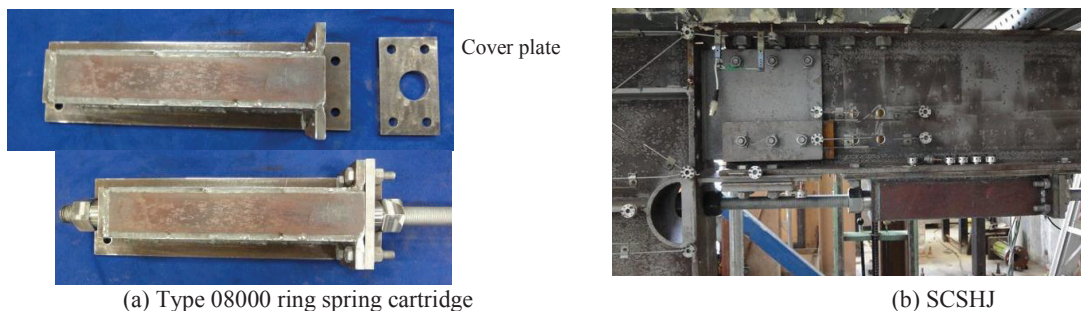


Figure 6.2. Test specimen

6.3. SCSHJ response

Fig. 6.3 presents the experimental moment-rotational ($M-\Theta_r$) behaviour of the standard SHJ, RSJ and the SCSHJs respectively. The SHJ results were comparable to tests undertaken by Clifton (2005) and MacRae et. al. (2010). They were essentially rigid till sliding commenced at approximately $\delta = 0.75\%$. They did not exhibit the theoretical two stage increase in resistance due to the bolts rotating and gradually taking up the frictional resistance which smear the double slip effect (MacRae et. al 2010).

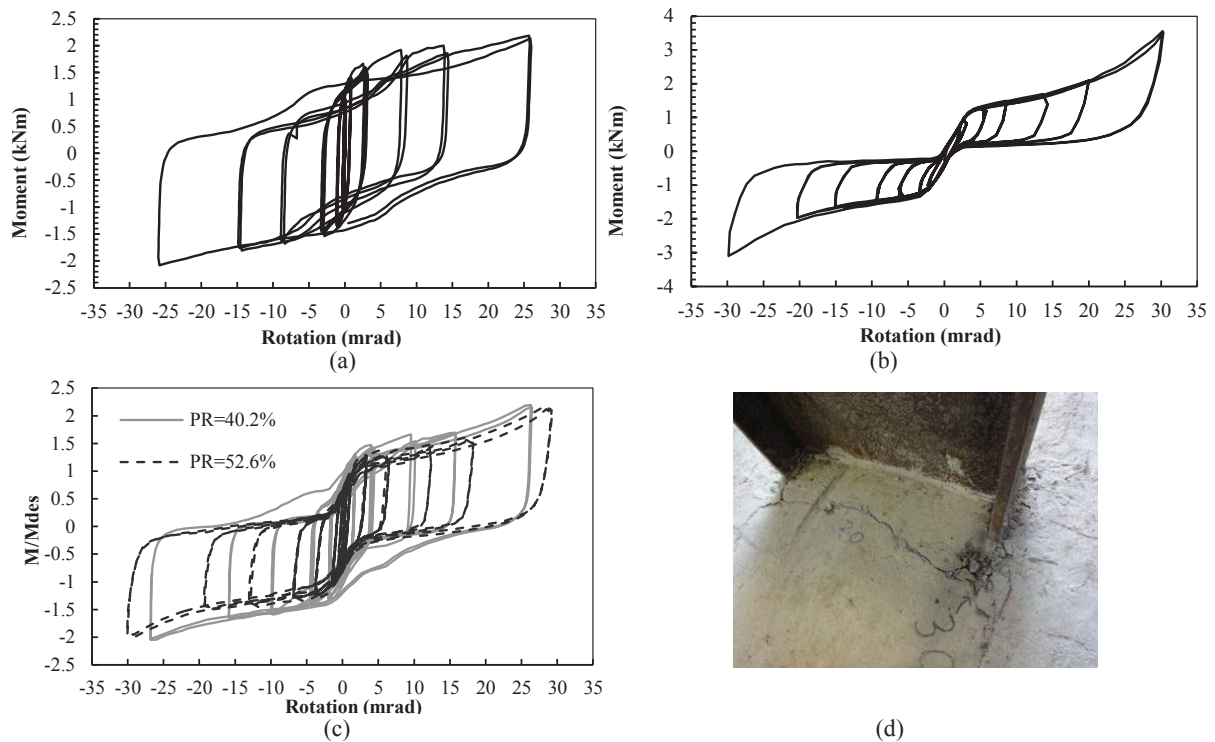


Figure 6.3. $M-\Theta_r$ (normalised by design moment) for (a) SHJ ,(b) RSJ, and (c) SCSHJ and (d) extent of slab damage after one test

The RSJ developed the stable, ideal flag-shaped self-centering behaviour. The initial elastic stiffness was observably lower due to flexibility of the threaded bar, and deformation between the threads in the bar and nuts. There was a definite yield moment where the ring spring started to compress. In the inelastic range, the ring spring cartridge performed as expected, compressing the springs during both positive and negative joint rotations, with the inelastic stiffness reasonably constant up to a rotation of 20 mrad. The SCSHJ behaviour displayed a combination of AFC and ring spring characteristics (Fig. 6.3c). They behaved as expected, with the curves better resembling the flag-shaped curve as P_{RS} increased. The rotational behaviour about the top flange plate was shown to be effective in isolating the floor slab. The damage was minimal, with largely hairline cracking on the surface of the slab. The extent of cracking around the column after the first test is shown in Fig. 6.3d.

7. SUMMARY AND CONCLUSIONS

This paper provided a review of the SHJ, AFC and SCSHJ developments. Due to space constraints, detailed analytical and experimental results were not discussed, but can be found in the references herein. The SHJ is a low-damage beam-column connection that confines inelastic demand to the bolts through the use of AFCs. The bolts can be tightened or replaced following a major earthquake. Abrasion resistant steel shims improved the performance of the AFC and was recommended for use in future construction. The AFC bolts are subject to interaction of moment-shear-axial forces, resulting in an uneven distribution of stress in the bolt cross-sectional area. The sliding shear capacity is therefore

determined by the model developed from plastic theory. The SCSHJ incorporates ring springs as a self-centering component. The ring spring is designed as a percentage of total joint moment capacity (P_{RS}), with analytical studies showing reduced frame residual drifts. The SCSHJ has been tested experimentally, showing improved flag-shape response with increasing P_{RS} .

ACKNOWLEDGEMENT

The authors would like to thank the New Zealand Earthquake Commission (EQC), Composite Floor Decks Ltd and Ringfeder GmbH for sponsorship, and Aurecon for details of the Te Puni Village Tower Building. All opinions expressed in this paper are those of the authors and do not necessarily represent those of the sponsor.

REFERENCES

- Bisalloy Steels (2008). Bisplate Technical Guide.
- Chanchi-Golondrino, J., MacRae, G., Chase, G., Rodgers, G., Mora-Munoz, A., Clifton, C. (2012). Design considerations for braced frames with asymmetrical friction connections - AFC. 7th STESSA Conference on the Behaviour of Steel Structures in Seismic Areas. Santiago, Chile.
- Clifton, C. (2005). Semi-rigid joints for moment-resisting steel framed seismic-resisting systems. Department of Civil and Environmental Engineering. Auckland, University of Auckland.
- Filiatrault, A., Tremblay, R. and Kar, R. (2000). "Performance Evaluation of Friction Spring Seismic Damper." *Journal of Structural Engineering* **126(4)**, 491-499.
- Gledhill, S. M., Sidwell, G. and Bell, D. (2008). The Damage Avoidance Design of tall steel frame buildings - Fairlie Terrace Student Accommodation Project, Victoria University of Wellington. Proceedings of the 2008 New Zealand Society for Earthquake Engineering: Engineering and Earthquake Resilient New Zealand. Taupo.
- Grigorian, C. E. and E. P. Popov (1994). Energy dissipation with slotted bolted connections. Berkeley, Calif., Earthquake Engineering Research Center.
- Khan, M. J. and Clifton, C. (2011). "Proposed development of a damage resisting eccentrically braced frame with rotational active links." *Bulletin of New Zealand Society of Earthquake Engineering* **44(2)**, 99-107.
- Khoo, H.H., Clifton, C., Butterworth, J., MacRae, G. and Ferguson, G. (2012a). "Influence of steel shim hardness on the Sliding Hinge Joint performance." *Journal of Constructional Steel Research* **72(0)**, 119-129.
- Khoo, H. H., Clifton, C., Butterworth, J. and MacRae, G. (2012b). Experimental studies of the self-centering Sliding Hinge Joint. New Zealand Society for Earthquake Engineering Conference. Christchurch, New Zealand.
- Khoo, H. H., Clifton, C., Butterworth, J. and MacRae, G. (2012c). "Development of the self-centering Sliding Hinge Joint with ring springs." *Journal of Constructional Steel Research* (under review).
- MacRae, G., Clifton C., Mackinven, H., Mago, N., Butterworth, J. and Pampanin, S. (2010). "The Sliding Hinge Joint Moment Connection." *Bulletin of New Zealand Society of Earthquake Engineering* **43(3)**, 202-212
- MacRae, G. A. and K. Kawashima (1997). "Post-earthquake residual displacements of bilinear oscillators." *Earthquake Engineering & Structural Dynamics* **26(7)**, 701-716.
- Ocel, J., DesRoches, R., Leon, R., Hess, G., Krumme, R., Hayes, J. and Sweeney, S. (2004). "Steel Beam-Column Connections Using Shape Memory Alloys." *Journal of Structural Engineering* **130(5)**, 732-740.
- Oyarzo-Vera, C.A., McVerry, G.H. and Ingham, J. (2012). "Seismic zonation and default suite of ground-motion records for time-sistory analysis in the North Island o New Zealand." *Earthquake Spectra* (In press)
- Ricles, J. M. and R. Sause (2001). "Post-tensioned seismic-resistant connections for steel frames." *Journal of Structural Engineering* **127(2)**, 113.
- Ringfeder GmbH (2008). Damping Technology. Krefeld, Germany.
- SAC Joint Venture (2000). Recommended design criteria for new steel moment frame structures. Rep. No. FEMA-350, for the Federal Emergency Management Agency. Washington, D.C.
- Standards New Zealand (2004a). NZS 1170.5:2004 - Structural design actions. Earthquake actions. 2004 ed. Wellington, New Zealand.
- Standards New Zealand (2009). NZS 3404:2009 – Steel structures standard. Wellington, New Zealand.